

Comparison of the potential energy for different equilibrium configurations of symmetric and asymmetric floating drops

Mason Mault* and Ray Treinen†

February 12, 2026

Abstract

We provide a numerical method for computing solutions to a free boundary problem arising from the equilibrium state of a floating drop. This numerical method is based on a Newton's method for the underlying nonlinear boundary value problems, and at each iterative step a Chebyshev spectral collocation method is employed. The problems considered here are those that can be described by using generating curves, and include problems in \mathbb{R}^2 and \mathbb{R}^3 .

The resulting nine-dimensional space of physical parameters is explored, and examples are given that highlight the potential energy of centrally located drops, wall-bound drops, and asymmetric configurations in \mathbb{R}^2 . Non-uniqueness of solutions to the corresponding Euler-Lagrange equations is displayed, and also strong evidence of non-uniqueness of energy minimizers is given.

Keywords. Capillarity, Floating drops, Non-uniqueness

Mathematics Subject Classification: Primary 35Q35; Secondary 76M22

1 Introduction

We consider the problem of finding the equilibrium state of three immiscible fluids in a laterally bounded container, sometimes known as a floating drop problem. A guiding example would be water rising in a capillary tube with a small drop of oil introduced to the system, as is shown in Figure 1. In every case,

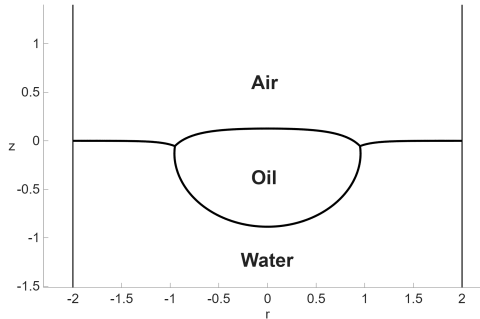


Figure 1: Schematically, a drop of oil floats on the surface of water inside a capillary tube. Shown is a vertical section of an axially symmetric configuration in \mathbb{R}^3 . The capillary tube is indicated by the two vertical lines, and the tube walls will be omitted in all other figures in this work.

*Department of Mathematics, Texas State University, 601 University Dr., San Marcos, TX 78666, mdm353@txstate.edu
 †Department of Mathematics, Texas State University, 601 University Dr., San Marcos, TX 78666, rt30@txstate.edu

we will find numerical solutions for these configurations are always non-unique, and we will also show many examples of symmetry breaking with a lower-energy state given by an asymmetric configuration. What is particularly striking is that some examples are found where the energy minimizer is not unique.

A little more detail is needed to be specific. Given a laterally bounded container partially filled by a fluid, we introduce a prescribed volume of a different fluid, known as the drop, and we consider here only drops with densities less than the density of the supporting fluid. As we will see in the next section, there are nine physical parameters of interest in this problem, and we explore this parameter space for examples that highlight the symmetry and asymmetry of the resulting configurations as well as other interesting phenomena. Our methods are computational, and not analytical, however we will comment on the limited theory as it currently sits. For any selection of physical parameters we find configurations where the drop is adjacent to the wall of the container, and we also find configurations with the drop floating in center of the container. There are examples of non-uniqueness of solutions to the resulting free boundary problems for every set of parameters we considered. We compute the potential energy of both configurations of the wall-bound drops and the centrally floating drops to determine which configuration has the lower energy. Surprisingly, there are many selections of parameters where the two configurations have the same potential energy. This is the first time non-uniqueness has been observed with this model of the physical configuration, both at the level of the competing floating drop configurations, as well as the configurations that produce energy minimizers.

Our approach to floating drop problems follows the framework established by Elcrat, Neel, and Siegel [8]. Historically, the mathematical study of three immiscible fluids in equilibrium goes back to at least 1806, when Laplace considered mercury on water [18]. Massari [22], Leonardi [20], Elcrat and Treinen [10], and Blank, Elcrat, and Treinen [4] studied floating drops using functions of bounded variation. In this direction, both Maggi [21] and Morgan [28] consider fluid clusters in their books, with further references therein. Ickes and Treinen [17] combined floating drops with additional floating rigid objects. Slobozhanin [30] contributed to the problem, and also see Gibbs [13] as a precursor for [8]. Treinen [33] gave a general existence theorem for symmetric configurations, then he established the symmetry of some configurations [35], and also see [37]. Lawlor and Morgan [19], Morgan [27], and White [39] treat three immiscible fluids using more general geometric measure theory. Numerical simulations were also done by Elcrat and Treinen [9], and that work can be seen as the approach we both improve upon and extend to new configurations here.

Physically, the appropriate approach is to study two-dimensional surfaces describing the boundaries between the fluids, and the fluids are described as subsets of \mathbb{R}^3 . We restrict our attention to those problems described by ordinary differential equations. For our first consideration this means that we are restricting our interfaces to be radially symmetric about a vertical axis. It would also be interesting to study the full three-dimensional problem without this symmetry, however that would require techniques beyond the scope of this project.

We will also consider the lower-dimensional model in \mathbb{R}^2 . The arguments in [8] that are used here do not depend on the underlying dimension of the problem. As we will see, our solutions also satisfy some ordinary differential equations, but we will be able to identify examples of symmetry breaking in this case. This type of configuration has a physical interpretation beyond the lower-dimensional analogue of the problem. If one considers two vertical plates at $y = \pm\epsilon$ for a small enough $\epsilon > 0$ and with homogeneous wetting energies on these vertical plates so that the contact angles are all $\pi/2$ there, then the floating drop problem will be a horizontal cylinder traced out by the lower-dimensional problem. Of course, if ϵ is allowed to be large, then the stability of these drops becomes unlikely. However, with this view in mind, we continue to refer to quantities of volume and area in both model problems.

In the next section the mathematical model and numerical methods are discussed, concluding with a discussion of the free parameters in these problems. Section 3 collects our experiments in \mathbb{R}^3 . Specifically, in Subsection 3.1 an example experiment is given where the volume of a drop is increased, and the resulting energy profiles of centrally located drops and wall-bound drops are compared. In Subsection 3.2

other examples in \mathbb{R}^3 are explored, following the general framework established for the different types of parameters. A heuristic is given for when a centrally located drop might tend to be the energy minimizer. In Section 4 floating drops in \mathbb{R}^2 are considered, with Subsection 4.1 collecting more overviews of parameter studies, and an example is given where the heuristic guide provided in Subsection 3.2 is false. Then in Subsection 4.2 the symmetry of energy minimizers is explored, and some asymmetrical configurations are highlighted. Finally, in Section 5 we summarize our conclusions.

Codes to produce the floating drops considered in this work can be found at
<https://github.com/raytreinen/Floating-Drops>

The first author was partially supported by the NSF Grant, DMS-2144232.

2 The mathematical model and basic algorithms

In this section we introduce the mathematical model. As the parameters involved in our approach naturally lead to a numerical algorithm, we discuss our numerical approach in the same exposition.

2.1 Energy and related parameters

We consider the interior of the capillary tube as a domain Ω , which is either as a subset of \mathbb{R}^2 or \mathbb{R}^3 that is laterally bounded, and $\partial\Omega$ extends vertically as an infinite cylinder or two vertical lines if $\Omega \subset \mathbb{R}^2$. Specifically, $\Omega = B \times \mathbb{R}$ for a ball B in \mathbb{R} or \mathbb{R}^2 . There are three fluids, represented by the sets E_0, E_1, E_2 that must satisfy $\bar{E}_0 \cup \bar{E}_1 \cup \bar{E}_2 = \bar{\Omega}$. The set E_1 represents the drop and has a finite volume, while the other two fluids have infinite volume. The boundaries of the fluids are assumed to be C^2 surfaces away from the triple junction, Γ , which we assume is a smooth curve in \mathbb{R}^3 , or either one or two triple-junction points in \mathbb{R}^2 , and we assume that the interfaces between any two of the fluids is C^1 up to Γ and $\partial\Omega$ as appropriate. These surfaces are not assumed to be graphs over B in general.

The interface between E_i and E_j is denoted by S_{ij} , where $S_{ij} = S_{ji}$. When convenient, we will use function notation for these surfaces, and when we do so, we fix u for S_{01} , v for S_{12} , and w for S_{02} . Associated to each surface is a surface tension: $\sigma_{01}, \sigma_{12}, \sigma_{02}$, giving a surface energy that can be written as the surface tension times the area of each surface. The force balance condition

$$\begin{aligned} \sigma_{01} &\leq \sigma_{12} + \sigma_{02}, \\ \sigma_{12} &\leq \sigma_{01} + \sigma_{02}, \\ \sigma_{02} &\leq \sigma_{01} + \sigma_{12} \end{aligned} \tag{1}$$

is assumed. This is necessary for equilibrium, as described in [4], [8], [10], and [22].

The contact angle between S_{ij} and S_{ik} is denoted by γ_{jk} . The contact angles and surface tensions must satisfy the Neumann triangle relation:

$$\frac{\sin \gamma_{01}}{\sigma_{01}} = \frac{\sin \gamma_{12}}{\sigma_{12}} = \frac{\sin \gamma_{02}}{\sigma_{02}}, \tag{2}$$

as proved in [8], and this is illustrated in Figure 2. Each fluid E_j has an associated density ρ_j and we only consider the case $\rho_0 \leq \rho_1 \leq \rho_2$. Then, for each fluid, the potential energy due to gravity is generically

$$\int_E \rho g z \, dV$$

with horizontal slices taken at each height z . We can iterate that integral so that we have $\int(\int_0^u z \, dz) = 0.5 \int(\text{sgn } u) u^2$ for a generic surface with height u , though the domain of the second integral depends on the geometry of the configuration and we will say more about this later. For now we note that this

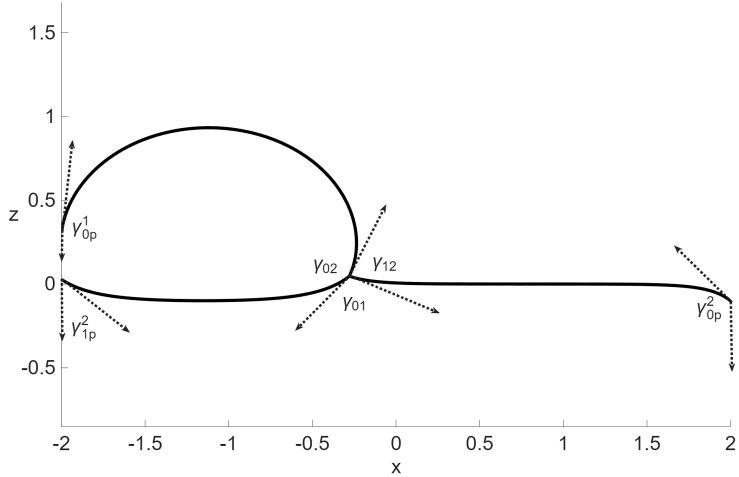


Figure 2: The surface tensions are shown in a force balance form as vectors, and the contact angles associated contact angles are shown. The plate angles are also shown. The floating drop pictured here is a wall-bound drop in \mathbb{R}^2 .

allows us to consider finite quantities for the gravitational potential energy in reference to a height $z = 0$. This reference level is based on the capillary tube being placed in an exterior bath of liquid E_2 , and that bath of liquid is unbounded, with the reference height for its interface given by a limiting height as the distance to the tube goes to infinity. Of course, we take a coordinate system so that this reference height is zero. Each surface has an associated capillary constant given by

$$\kappa_{01} = g \frac{\rho_1 - \rho_0}{\sigma_{01}}, \quad \kappa_{12} = g \frac{\rho_2 - \rho_1}{\sigma_{12}}, \quad \kappa_{02} = g \frac{\rho_2 - \rho_0}{\sigma_{02}}, \quad (3)$$

and we normalize this with the assumption that $\rho_0 = 0$.

The final component is a wetting energy, and this quantity drives the fluid rise of a meniscus in a tube. Here we borrow our terminology from the sessile drop technique for measuring contact angles where a drop of fluid is placed on a horizontal plate. Interestingly, this technique goes back to Adams and Bashforth and their multi-step method [3]. If we take a convention on labeling the contact angles at the wall by using the super-script to indicate the set on whose interior the angle is measured, and the subscript contains the labels showing the adjacent fluid and that this is a “plate” angle. The wetting energy is a constant multiplied by the surface area of the tube in contact with a given fluid, but since that is infinite for two of the liquids in our model, we simply use the reference height of zero so that wetted areas corresponding to negative heights give negative surface area. Then, using the variational argument found in Finn [11], or more pertinent, his paper [12], Elerat, Neel, and Siegel [8], Maggi [21], or McCuan and Treinen [25], we can relate $\cos \gamma_{1p}^2$ to the other angles. Take note that the wetting coefficient of E_1 is $-\sigma_{01} \cos \gamma_{0p}^1$ and the wetting coefficient of E_2 is $-\sigma_{02} \cos \gamma_{0p}^2$, and then, using Finn’s derivation [12],

$$\sigma_{12} \cos \gamma_{1p}^2 = -\sigma_{01} \cos \gamma_{0p}^1 + \sigma_{02} \cos \gamma_{0p}^2. \quad (4)$$

We will use two of these plate angles to derive the third, and we choose a particular pair depending on what is motivating the experiment at the time. These contact angles are also depicted in Figure 2.

Floating drops may be seen as critical points or (local) minimizers of the energy functional

$$\begin{aligned}\mathcal{E} := & \sigma_{01}|S_{01}| + \sigma_{02}|S_{02}| + \sigma_{12}|S_{12}| + \sum_{i=0}^2 \rho_i g \int_{E_i} z \, dV \\ & - \sigma_{01} \cos \gamma_{0p}^1 |\partial E_1 \cap \partial \Omega| - \sigma_{02} \cos \gamma_{0p}^2 |\partial E_2 \cap \partial \Omega|.\end{aligned}\quad (5)$$

2.2 Boundary value problems and a Chebyshev spectral collocation method

It was shown in [8] by a variational argument that the interfaces satisfy the following Young-Laplace equations and free boundary condition:

$$2H_{S_{01}}(x, y, z) = \kappa_{01}z + \lambda/\sigma_{01}, \quad (6)$$

$$2H_{S_{12}}(x, y, z) = \kappa_{12}z - \lambda/\sigma_{12}, \quad (7)$$

$$2H_{S_{02}}(x, y, z) = \kappa_{02}z, \quad (8)$$

$$S_{01}, S_{12}, S_{02} \text{ meet at } \Gamma \text{ and satisfy (2).} \quad (9)$$

Here $H_S(x, y, z)$ is defined to be the mean curvature of the surface S when $(x, y, z) \in S$ and is undefined otherwise. Often $z = z(x, y)$, then $2H_S(x, y, z) = \nabla \cdot Tz$ with $Tz = \nabla z / \sqrt{1 + |\nabla z|^2}$, though we will not assume this non-parametric form here. From this point onward, we will use the convention of capitalizing the height of the solutions of the differential equations without a Lagrange multiplier, and lower case letters will be reserved for the height of the physical interfaces.

Two particular forms of the differential equation $2H_U = \kappa U$ will sometimes be used. The first form assumes the solution in \mathbb{R}^3 is symmetric about the vertical axis, parametrized by arc length s , and is

$$\frac{dr}{ds} = \cos \psi, \quad (10)$$

$$\frac{dU}{ds} = \sin \psi, \quad (11)$$

$$\frac{d\psi}{ds} = \kappa U - \frac{\sin \psi}{r}. \quad (12)$$

Here r is the radial coordinate of the solution, U is the height, and ψ is the inclination angle measured from the positive radial axis. This form allows for inflection points and vertical points, where they exist. The next form is for solutions in \mathbb{R}^2 , and is similar:

$$\frac{dx}{ds} = \cos \psi, \quad (13)$$

$$\frac{dU}{ds} = \sin \psi, \quad (14)$$

$$\frac{d\psi}{ds} = \kappa U, \quad (15)$$

where the horizontal component of interface graph is x .

The appropriate boundary conditions for these systems of ODEs are to prescribe the inclination angle $\psi = \psi_b \in [-\pi, \pi]$ at some radius $r = b$ (or $x = b$). If the surface spans the vertical axis, then we prescribe $\psi = -\psi_b$ at $r = -b$, and these interfaces are well studied, with Finn [11] being an excellent reference for the system in \mathbb{R}^3 . If instead the surface is topologically annular, then we alternatively prescribe $\psi = \psi_a \in [-\pi, \pi]$ and $r = a$ for some $0 < a < b$. These annular capillary surfaces are not as well understood. In \mathbb{R}^3 , the papers by Elcrat, Kim, and Treinen [7], Gordon and Siegel [14], [15], Siegel [29], and Treinen [34] collect the theory as we know it, and Bagley and Treinen [2] present a united

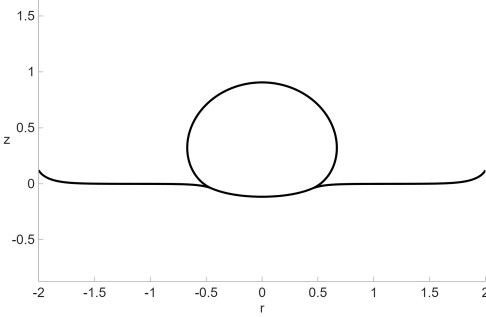


Figure 3: A typical centrally located floating drop. The physical parameters that determine this drop are a volume of 1, tube radius of $R = 2$, densities $\rho_1 = 1$ and $\rho_2 = 15$, surface tensions $\sigma_{01} = 6$, $\sigma_{02} = 2.0001$, and $\sigma_{12} = 7.9999$, and plate angle $\gamma_{0p}^2 = 0.5$.

approach. In \mathbb{R}^2 the surface (curve) is independent of horizontal translation, and is only fixed by the difference between a and b . The papers by McCuan [23], [24], McCuan and Treinen [26], and Wente [38] collect at least most of the relevant theory.

The basic idea is to use the systems of differential equations without Lagrange multipliers and solve boundary value problems over some domain with free boundary Γ and appropriate physical conditions for ψ there so that the interfaces U and V that correspond to S_{01} and S_{12} are (generally) positive.

We use the Chebyshev spectral collocation methods developed for these equations by Treinen [36]. These methods follow the rectangular collocation techniques of Driscoll and Hale [5] and the general overview by Aurentz and Trefethen [1]. Also see Trefethen [31]. These methods use a Newton method to treat the non-linearity of the equations, Chebyshev spectral methods to solve the resulting iterated linear systems, a scaling trick to compute the total arc-length of the solution of the boundary value problem as part of the system, and a continuity method for solutions that are not a graph over the base domain. The algorithm is adaptive and the tolerances are set to be within 14 digits of relative error for the Newton step and ten digits of the relative error for the boundary value problem. The programs used will then generate data points generically along (r, U, ψ) associated with a number of Chebyshev points on an interval of length 2ℓ , which is the total arc-length of the generating curve. This is typically achieved with $n + 1 = 14$ Chebyshev points. We refer the reader to [36] for more details. This approach is robust and is a significant improvement over the sometimes unstable shooting methods used in [9], though it should be pointed out that there are extreme cases where the algorithm used here could fail to converge, even when modified to localize problematic portions of the solution curve using domain decomposition, as is discussed by Haug and Treinen [16]. In our experiments for this work we have called this solver millions of times and have never encountered the degenerate cases that were explored in [16]. From this point onward, when we mention solutions to a particular boundary value problem, we mean a numerical approximation that is found with the algorithm from [36] using the tolerances we have mentioned above.

2.3 Matching physical surfaces

Next, we note that in [8] the Lagrange multiplier λ was eliminated by matching the interfaces at the free boundary Γ , which is at a particular radius $r = \bar{r}$, and they found

$$\lambda = (\bar{U} + \bar{V}) \frac{\kappa_{01}\sigma_{01}\kappa_{12}\sigma_{12}}{\kappa_{01}\sigma_{01} + \kappa_{12}\sigma_{12}} \quad (16)$$

with \bar{U} and \bar{V} representing the heights at \bar{r} . The same formula holds for the lower dimensional model with $x = \bar{x}$. Then eliminating λ results in physical interfaces

$$u = \frac{\lambda}{\kappa_{01}\sigma_{01}} - U \quad (17)$$

$$v = V - \frac{\lambda}{\kappa_{12}\sigma_{12}} \quad (18)$$

that match at \bar{r} (or \bar{x}). With the surfaces u and v matched at some fixed $\bar{r} > 0$ (or $\bar{x} > 0$), we do not in general have $w = u = v$ there.

Before proceeding to match $w = u = v$ at \bar{r} , we need to describe the geometry of the interfaces near the free boundary. To fix the concepts, consider first a centrally located drop that is symmetric about the vertical axis, as shown in Figure 3. Then the boundary conditions on v depend on the inclination of v at \bar{r} . We denote this crucial quantity by $\bar{\psi}$, and the boundary conditions for v are then that the inclination angle of that surface is $-\bar{\psi}$ at $r = -\bar{r}$ and $\bar{\psi}$ at $r = \bar{r}$. Then we can use (2) and the surface tension values to formulate boundary conditions for u based on $\bar{\psi}$. Figure 2 is a useful companion for deriving these boundary conditions. It follows that U has inclination angles $-(\gamma_{02} - \bar{\psi})$ at $-\bar{r}$ and $\gamma_{02} - \bar{\psi}$ at \bar{r} . We also have an inclination angle of $\bar{\psi} + \gamma_{01} - \pi$ for w at \bar{r} , and w satisfies $\sin \psi = \cos \gamma_{0p}^2$ at $r = R$.

Then we note that $\bar{\psi} = 0$ gives $V \equiv 0$ and $v < 0$ while w positive at \bar{r} , which can be proved in many cases, but is in general merely an observed fact. The conditions on these component interfaces were discussed in [33]. Then when $\bar{\psi} = \gamma_{02}$, $U \equiv 0$ and $u > 0$, while w is (observed to be) negative at \bar{r} . Thus defining $\bar{v}(\bar{\psi})$ and $\bar{w}(\bar{\psi})$ to be the heights of v and w at \bar{r} for a particular $\bar{\psi}$, we can then define

$$F(\bar{\psi}) := \bar{v}(\bar{\psi}) - \bar{w}(\bar{\psi}) \quad (19)$$

and we observe that there is some value of $\bar{\psi} \in (0, \gamma_{02})$ that is a zero of F . We find this value of $\bar{\psi}$ numerically using Matlab's fzero function applied to $F(\bar{\psi})$ with an initial guess of $\bar{\psi} = \gamma_{02}/2$. The tolerance of Matlab's fzero algorithm defaults to near machine precision. The repeated calls to $F(\bar{\psi})$ will generate surfaces u , v , and w for each attempted value of $\bar{\psi}$, so the spectral solver is used multiple times inside this fzero process.

Then with this critical value of $\bar{\psi}$, we have matched u , v , and w at a prescribed $\bar{r} > 0$.

2.4 Drop volumes

In general, the enclosed volume of the drop just formed will not match the prescribed volume of the drop. What remains in the floating drop problem is to match the prescribed volume.

In order to efficiently compute the volume, we derive two volume formulas, depending on whether the drop is centrally located or bound to the wall. First we find an identity for a generic (r, V, ψ) solution to (10)-(12):

$$\begin{aligned} \frac{d}{ds} (r \sin \psi) &= \cos \psi \sin \psi + r \cos \psi \left(\kappa u V - \frac{\sin \psi}{r} \right) \\ &= \kappa r V \cos \psi. \end{aligned} \quad (20)$$

Then the centrally located drop is made up of two volumes of fluid, divided by the horizontal plane $z \equiv \bar{v}$. We will compute the two component volumes Vol_U and Vol_V using the standard representation,

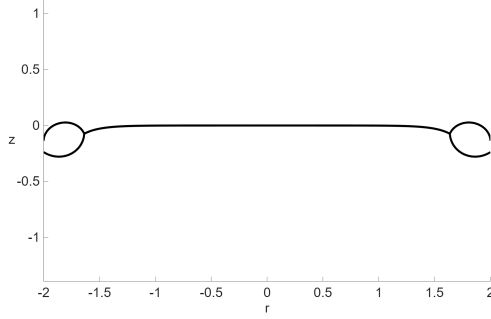


Figure 4: A typical wall-bound floating drop. The physical parameters that determine this drop are a volume of 1, tube radius of $R = 2$, densities $\rho_1 = 14$ and $\rho_2 = 15$, surface tensions $\sigma_{01} = 6.01$, $\sigma_{02} = 2.99$, and $\sigma_{12} = 7$, and plate angles $\gamma_{0p}^1 = \pi - 0.01$ and $\gamma_{1p}^2 = 1$.

which is merely a rigid motion of the physical component volumes. Then

$$\begin{aligned}
 \text{Vol}_V &= 2\pi \int_0^{\bar{r}} (\bar{V} - V) r dr \\
 &= \pi \bar{V} \bar{r}^2 - \int_0^{\bar{r}} \rho V \frac{dr}{ds} ds \\
 &= \pi \bar{V} \bar{r}^2 - \frac{2\pi}{\kappa_{12}} \int_0^{\bar{r}} \frac{d}{ds} (r \sin \psi) ds \\
 &= \pi \bar{V} \bar{r}^2 - \frac{2\pi}{\kappa_{12}} \bar{r} \sin \bar{\psi}
 \end{aligned} \tag{21}$$

and similarly

$$\text{Vol}_U = \pi \bar{U} \bar{r}^2 - \frac{2\pi}{\kappa_{01}} \bar{r} \sin (\gamma_{02} - \bar{\psi}). \tag{22}$$

We obtain the total volume of $\text{Vol} = \text{Vol}_U + \text{Vol}_V$ for the centrally located drop. We have chosen to present a cleaner partial derivation that assumes the interfaces do not continue past $\bar{\psi} = \pi/2$, though the same formula holds for those larger $\bar{\psi}$ values as well. We also note that if either of the interfaces U or V passes above the corresponding \bar{U} or \bar{V} , then that portion of the volume will be negative. However, the other interface will be adding exactly that missing volume to the total. We will also exclude any non-physical drops where u and v intersect away from \bar{r} .

Then we have a second fzero module where we match the computed volume to the prescribed volume by varying \bar{r} . The initial guess for \bar{r} is generally $0.2\sqrt[3]{\text{Vol}}$, but the factor of 0.2 may need to be adjusted in some cases. In some of the automation that will follow in this paper, this factor may need to be changed adaptively. The output of these two nested loops gives a solution to the floating drop problem with a centrally located drop.

To compute radially symmetric wall-bound drops in \mathbb{R}^3 , recall that the drop forms a ring around the edge of the wall, and we work with a section of this radially symmetric configuration, as is shown in Figure 4. We adapt the above process to the left side of the configuration, where the generating curves start at radius $-R$ and the upper and lower portions of the drop meet at $-\bar{r}$. Starting with the lower interface V , this interface has inclination angles $\gamma_{1p}^2 - \frac{\pi}{2}$ at $r = -R$ and $\bar{\psi}$ at $r = -\bar{r}$ with $\bar{\psi} \in (0, \gamma_{02})$. Then U has inclination angle $\frac{\pi}{2} - \gamma_{0p}^1$ at $r = -R$ and $\gamma_{02} - \bar{\psi}$ at $r = -\bar{r}$. Finally, w has inclination angle $\bar{\psi} + \gamma_{01} - \pi$ at $r = -\bar{r}$ and $-(\bar{\psi} + \gamma_{01} - \pi)$ at $r = \bar{r}$.

As before, we take rigid motions of U and V to match the interfaces at $r = -\bar{r}$ using the Lagrange multiplier λ to obtain the physical surfaces denoted by u and v . Then when evaluated at $r = \bar{r}$, \bar{v} in

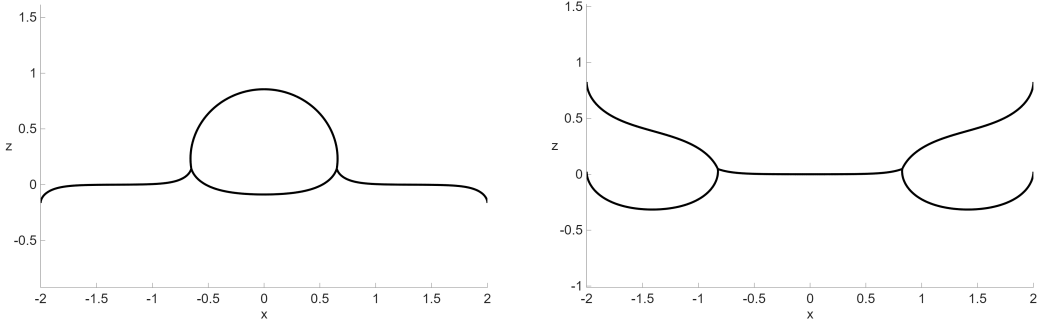


Figure 5: Displayed are analogues of the symmetric floating drops in \mathbb{R}^2 . On the left is a centrally located drop with the physical parameters that determine this drop being a volume of 1, tube radius of $X = 2$, densities $\rho_1 = 0.4$ and $\rho_2 = 15$, surface tensions $\sigma_{01} = 7.9$, $\sigma_{02} = 2$, and $\sigma_{12} = 6.1$, and plate angle $\gamma_{0p}^2 = \pi - 0.01$. On the right is a wall-bound drop with the physical parameters that determine this drop being a volume of 1.5 split evenly on each wall, tube radius of $X = 2$, densities $\rho_1 = 7.5$ and $\rho_2 = 15$, surface tensions $\sigma_{01} = 7.5$, $\sigma_{02} = 2.5$, and $\sigma_{12} = 6$, and plate angles $\gamma_{0p}^1 = 0.01$ and $\gamma_{1p}^2 = 0.01$.

general is not equal to \bar{w} in this case either, so a similar $F(\bar{\psi})$ is constructed here, and a zero is found numerically using Matlab's fzero.

As in the earlier case, with this critical value of $\bar{\psi}$, we have matched u , v , and w at a prescribed $\bar{r} > 0$. As before, in general, the enclosed volume of the drop just formed will not match the prescribed volume of the drop.

To compute the enclosed volume for the drop bound to a wall, following the above computation, we obtain

$$\text{Vol}_V = \pi \bar{V} (R^2 - \bar{r}^2) - \frac{2\pi}{\kappa_{12}} \left(R \sin \left(\frac{\pi}{2} - \gamma_{1p}^2 \right) - \bar{r} \sin(-\bar{\psi}) \right), \quad (23)$$

where we use $-\bar{\psi}$ at \bar{r} as the angle there is derived from the left side of the drop, though the volume is more naturally derived from the right side. We also have

$$\text{Vol}_U = \pi \bar{U} (R^2 - \bar{r}^2) - \frac{2\pi}{\kappa_{01}} \left(R \sin \left(\gamma_{0p}^1 - \frac{\pi}{2} \right) - \bar{r} \sin(\bar{\psi} - \gamma_{02}) \right). \quad (24)$$

also giving the form $\text{Vol} = \text{Vol}_U + \text{Vol}_V$ in this case.

Then we again have a second fzero module where we match the computed volume to the prescribed volume by varying \bar{r} . The output of these two nested loops gives a solution to the floating drop problem with a wall-bound drop.

2.5 Floating drops problems in \mathbb{R}^2

The above processes can also be carried out for \mathbb{R}^2 . We will have more cases to consider here. Of course, we have the centrally located drop and the analogue of the symmetric wall-bound drop as above which is actually two drops of equal volume, each of which is bound to an opposing wall, and these are shown in Figure 5. We are not restricted to symmetric interfaces here, as asymmetric configurations are possible to compute. One such configuration being a wall-bound to a single wall, and we can also have split drops with different volumes of the drop attached to each wall, and these are shown in Figure 6.

There may be other configurations possible, but those are the ones we consider in this work. The notation changes so that the boundary of the container at $x = -X$ and $x = X$, and the free boundary is located at $x = \pm \bar{x}$ for the centrally located drop, or some $x = \bar{x}$ generically otherwise. The main

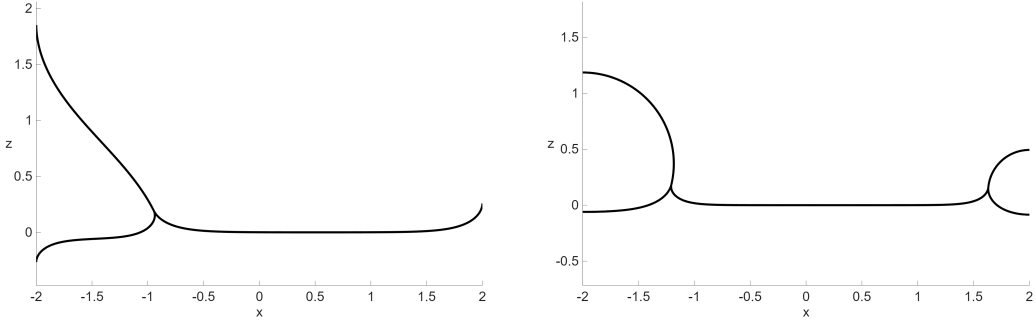


Figure 6: Asymmetric floating drops in \mathbb{R}^2 . On the left is a drop adjacent to the left wall with the physical parameters that determine this drop being a volume of 1, tube radius of $X = 2$, densities $\rho_1 = 1, \rho_2 = 15$, surface tensions $\sigma_{01} = 7.9999, \sigma_{02} = 5$, and $\sigma_{12} = 3.0001$, and plate angles $\gamma_{0p}^1 = 0.01$ and $\gamma_{1p}^2 = \pi - 0.01$. On the right is a drop split with $1/6$ of the volume of liquid adjacent to the right wall, and the remaining volume of fluid adjacent to the left wall. The physical parameters are a total volume of 1, tube radius of $X = 2$, densities $\rho_1 = 0.01$ and $\rho_2 = 15$, surface tensions $\sigma_{01} = 7.9999, \sigma_{02} = 2.0001$, and $\sigma_{12} = 6$, and plate angles $\gamma_{0p}^2 = \pi/2$ and $\gamma_{1p}^2 = \pi/2$.

changes are the volume formulas, where the components become

$$\begin{aligned} \text{Vol}_V &= 2 \int_0^{\bar{x}} (\bar{V} - V) \, dx \\ &= 2\bar{x}\bar{V} - \frac{2}{\kappa_{12}} \int_0^{\ell} \frac{d\psi}{ds} \frac{dx}{ds} \, ds \\ &= 2\bar{x}\bar{V} - \frac{2}{\kappa_{12}} \sin \bar{\psi}, \end{aligned} \quad (25)$$

$$\text{Vol}_U = 2\bar{x}\bar{U} - \frac{2}{\kappa_{01}} \sin (\gamma_{02} - \bar{\psi}), \quad (26)$$

for the central drop. For the wall-bound drop on the right we have

$$\text{Vol}_V = \int_{\bar{x}}^X (\bar{V} - V) \, dx = (X - \bar{x})\bar{V} - \frac{1}{\kappa_{12}} \left(\sin \left(\frac{\pi}{2} - \gamma_{1p}^2 \right) - \sin (-\bar{\psi}) \right), \quad (27)$$

and

$$\text{Vol}_U = (X - \bar{x})\bar{U} - \frac{1}{\kappa_{01}} \left(\sin \left(\gamma_{0p}^1 - \frac{\pi}{2} \right) - \sin (\bar{\psi} - \gamma_{02}) \right), \quad (28)$$

and for a wall-bound drop on the left where the interfaces span from $x = -X$ to the free boundary at $x = \bar{x}$, we have

$$\text{Vol}_V = (\bar{x} + X)\bar{V} - \frac{1}{\kappa_{12}} \left(\sin \bar{\psi} - \sin \left(\gamma_{1p}^2 - \frac{\pi}{2} \right) \right), \quad (29)$$

and

$$\text{Vol}_U = (\bar{x} + X)\bar{U} - \frac{1}{\kappa_{01}} \left(\sin (\gamma_{02} - \bar{\psi}) - \sin \left(\frac{\pi}{2} - \gamma_{0p}^1 \right) \right). \quad (30)$$

Of course, if there is a split drop that has a volume attached to each wall, we can use these formulas to compute those volumes. This split drop has two different free boundary triple junction points, and they are varied independently to achieve the prescribed volume on each side of the container.

2.6 Parameter discussion

In this section we have discussed the model of a floating drop, and there are a number of parameters that match the model to a particular physical configuration. The list of the nine available parameters is Vol , the volume of the drop, the container size indicated by R or X , the two densities ρ_1 and ρ_2 , the three surface tensions σ_{01} , σ_{02} , and σ_{12} , and the two free wetting energies $-\sigma_{01} \cos \gamma_{0p}^1$ and $-\sigma_{02} \cos \gamma_{0p}^2$. Since our model only relies on the difference in the densities, we are able to assume $\rho_0 = 0$, and we also use the dependence of the third wetting energy $\sigma_{12} \cos \gamma_{1p}^2$ on the two free wetting energy parameters. Our treatment of these parameters is decidedly abstract, and we make no attempt to fit our solutions to experimental data. We do explore this nine-dimensional parameter space in what follows. In the next section, we start with an example that is potentially experimentally reproducible by increasing the volume of the drop. In the remainder of the paper we will focus on other parameter studies that we found to give interesting results. In our time working with these problems, we have found that there are four groupings of parameters. The bulk parameters are the container size and the drop volume, and we have chosen to fix $R = 2$ and $X = 2$ while varying the drop volume. The two terms related to the gravitational energy are seen in the two densities, and we fix $\rho_2 = 15$ and consider a variety of choices of ρ_1 . The contact angles at the triple junction free boundary (boundaries) are derived by the three surface tensions, and we arbitrarily normalize these to add up to a value of 16. We often choose values of surface tensions to get γ_{02} near π , as we have found such edge cases make more striking examples. Finally, the wetting energies do depend on the surface tensions, but (4) allows us to fix two plate contact angles to derive the third. While we report both typical and interesting cases of the explorations we have made into this somewhat large parameter space, there are complicated interactions between the parameters, and we make no claim that we have exhausted all of the interesting cases.

3 Floating drops in \mathbb{R}^3

Here we discuss the remaining details needed to formulate the potential energy for configurations in \mathbb{R}^3 . We also explore an example that illustrates a process that could lead to a physical experiment for verification of our results, and then we give some examples from our basic groups of physical parameters as well as an interesting geometrical symmetry in the parameter space.

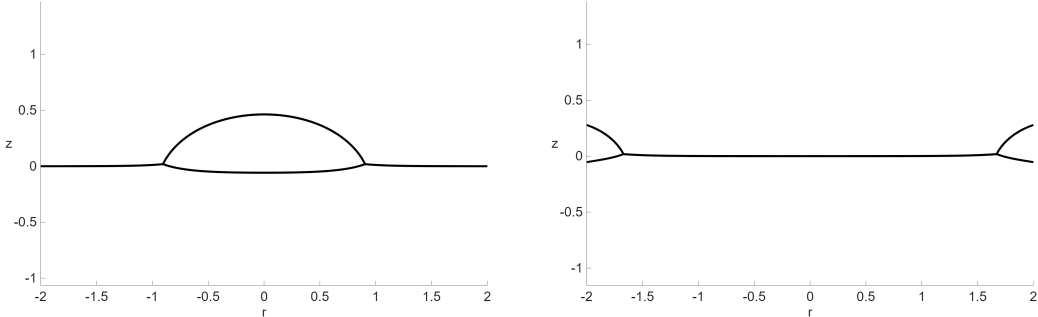


Figure 7: A pair of axially symmetric floating drops with the same parameters and a volume of 0.8. The potential energy of the wall-bound drop is lower than that of the centrally located drop. The physical parameters that determine these drops are a tube radius of $R = 2$, densities $\rho_1 = 1$ and $\rho_2 = 15$, surface tensions $\sigma_{01} = 3$, $\sigma_{02} = 7$, and $\sigma_{12} = 6$, and plate angles $\gamma_{0p} = \pi/2$, and $\gamma_{1p}^2 = 1.73324$.

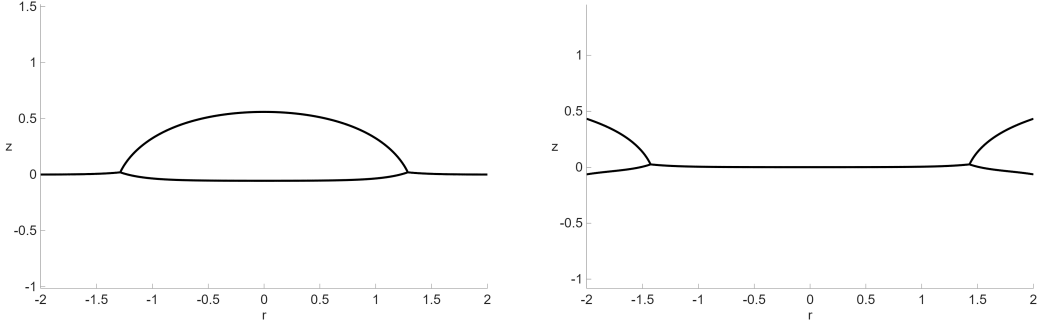


Figure 8: A similar pair of axially symmetric floating drops with the same parameters as those in Figure 7, except the drop volume is increased to 2. The potential energy of the centrally located drop is lower than that of the wall-bound drop.

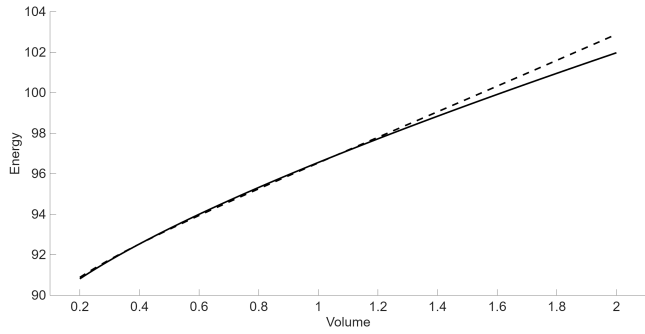


Figure 9: Comparing the energies of the centrally located drop (solid) and the wall-bound drop (dashed).

3.1 An example suitable for physical verification

In Figure 7 there are two different floating drop configurations that have the same parameters and a prescribed volume of 0.8. One drop is centrally located and the other is bound to the wall of the cylindrical container, and both are radially symmetric, giving an example of the non-uniqueness of the floating drop problem. In every choice of elements in our parameter space that we tested we have observed this non-uniqueness. Since both configurations are solutions to the Euler Lagrange equations as detailed above, the natural question is to determine the configuration with lower energy.

We need some details of how to compute the energy, which we will turn to shortly. First, we observe that the resulting energy of the centrally located drop is 95.322 and the energy of the wall-bound drop is 95.2593, so the wall-bound drop achieves a lower potential energy. Then in Figure 8 the situation is reversed, while the parameters remain the same except the drop volume is increased to 2, and the energy of the centrally located drop is 101.9708 however the energy of the wall-bound drop is 102.8821 and the centrally located drop achieves a lower potential energy.

In computing the potential energy for these configurations, there are terms for the surface area, gravitational potential, and wetting. To compute the surface areas of the component interfaces in \mathbb{R}^3 , we observe that the standard formula gives

$$S = 2\pi \int_a^b r ds \quad (31)$$

for solutions to the ODEs for some a and b when $r > 0$. If the interface does not intersect the vertical axis, then we simply set $a = 0$ and $b = 2\ell$ which is the total arc-length of our generating curve. Since we

have computed the solution r using Chebyshev points, it is natural to use a Clenshaw-Curtis quadrature to compute these integrals. Chebfun [6] is used to build the weights for these nodes. See Trefethen [32] for a discussion of the error bounds on these approximations. We will say that in our case there are $n + 1 = 14$ Chebyshev points in a typical surface, and the error of an $(n + 1)$ -point Clenshaw-Curtis quadrature I_n for the approximation of the integral $I = \int f(z) dz$ satisfies

$$|I - I_n| \leq \frac{64}{15} \frac{M \rho^{1-n}}{\rho^2 - 1} \quad (32)$$

for some M with the integrand $|f(z)| \leq M$, and ρ from the associated Bernstein ellipse E_ρ . If our surface spans the axis of symmetry, then we compute

$$S = \pi \int_{-\ell}^{\ell} |r| ds \quad (33)$$

using a halved double cover and the weights applied across the whole section, which is where we have our Chebyshev points.

Similarly, the gravitational potential energy of an interface w that spans the vertical axis is given by

$$G = 2\pi \int_0^{\bar{r}} \rho g \operatorname{sgn}(w) r w^2 dr = 2\pi \int_0^{\ell} \rho g \operatorname{sgn}(w) r w^2 \cos \psi ds, \quad (34)$$

for an appropriate density ρ , and with the usual $\operatorname{sgn}(w)$ function indicating the sign of w so that the gravitational potential is measured with respect to the reference level. This formula is derived here for the case when w is a graph over B , however, the arc-length form extends to parametric configurations that are not graphs over B .

These formulas are given generically, and are readily adapted to each component interface in our centrally located and wall-bound configurations.

The wetting energy for any surface is taken to be above or below the reference height $z \equiv 0$. If a fluid wets the wall, the wetting energy is simply the interface height on the boundary multiplied by $2\pi R$ and the relevant weight for that fluid.

With these details established, and motivated by the examples in Figures 7 and 8, we can now describe an experiment that could be physically conducted. We start with a small drop volume that is centrally located and continuously inject more volume into the drop, and while we increase the volume we measure the energy of the configuration. Then we repeat this process for the symmetric wall-bound drop. The results are collected in Figure 9. A careful view of this figure shows that there are two volumes where the centrally located drop has the same potential energy as the wall-bound drop. This is the first time there has been observed non-uniqueness of (presumed) energy minimizers in the floating drop problem. Of course, there are also possibly non-symmetric solutions to the floating drop problem, and we have not produced those examples here.

3.2 More examples

Next, we turn to the question of the balance between the gravitational potential energy and wetting energies. A guiding heuristic is that if the capillary tube configuration without a drop added gives an interface that is concave up, which means $0 < \gamma_{0p}^2 < \pi/2$, then adding a drop will lead to a centrally located drop as the energy minimizer. The physical reasoning is that the drop will descend to the bottom of the interface S_{02} in order to reduce the gravitational potential. The converse of this is when the interface is concave down and $\pi/2 < \gamma_{0p}^2 < \pi$ and then the heuristic is that the wall-bound drop would be the energy minimizer. We see these ideas in Figure 10, where the centrally located drop has

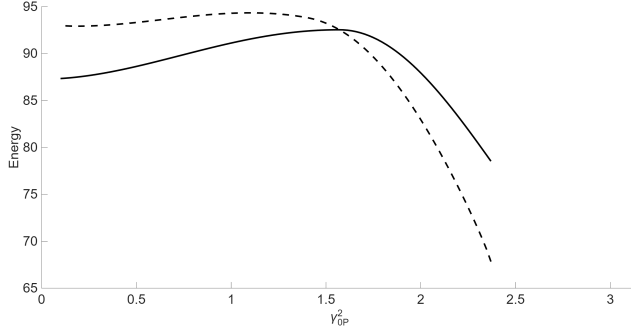


Figure 10: Comparing the energies of the centrally located drop (solid) and the wall-bound drop (dashed) in \mathbb{R}^3 . The physical parameters are a volume of 0.4 with tube radius $R = 2$, densities $\rho_1 = 1$ and $\rho_2 = 15$, surface tensions $\sigma_{01} = 3, \sigma_{02} = 7$, and $\sigma_{12} = 6$, plate angle $\gamma_{0p}^1 = 1.24139754239$.

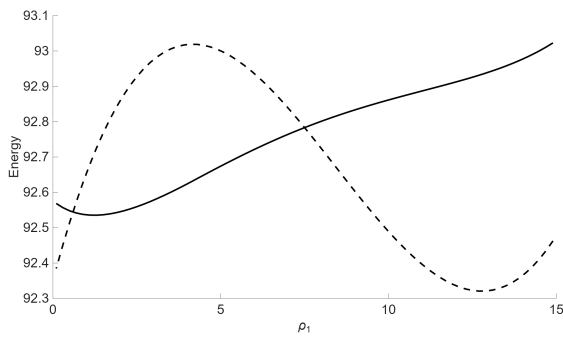


Figure 11: Comparing the energies of the centrally located drop (solid) and the wall-bound drop (dashed). The physical parameters are a volume of 0.4 with tube radius $R = 2$, density $\rho_2 = 15$, surface tensions $\sigma_{01} = 3, \sigma_{02} = 7$, and $\sigma_{12} = 6$, plate angles $\gamma_{0p}^2 = \pi/2$ and $\gamma_{1p}^2 = 1.727954$.

lower energy for all γ_{0p}^2 smaller than $\pi/2$, and when $\gamma_{0p}^2 > \pi/2$ the wall-bound drop has the smaller value of energy. We will pick this topic up again in Section 4.

In Figure 11 we show an experiment where the density of the drop is increased from $\rho_1 = 0$ to $\rho_1 = \rho_2 = 15$. Here there are two values of ρ_1 where the energy values are the same, and this is quite common in our parameter studies in \mathbb{R}^3 . In this experiment and many that follow, we focus on the neutrally wetting case where $\gamma_{0p}^2 = \pi/2$ and there is no driving concavity of the fluid in the tube without a drop present.

The fourth type of groupings of the energy terms would be the surface tensions themselves. We save an experiment involving γ_{02} for Section 4 as our explorations have not turned up a difference in the dimension of the problem for experiments of this type.

We do, however, finish our discussion of drops in \mathbb{R}^3 with a general observation on the symmetry of the geometry of the drops with respect to a certain symmetry in the parameters. Given fixed $\gamma_{0p}^2 = \pi/2$ and any admissible σ_{02} , as well as any admissible volumes, tube widths, densities ρ_2 , then if the surface tensions $\sigma_{01} = a$ and $\sigma_{12} = b$ are also admissible, and the density $\rho_1 = d \in [0, \rho_2]$, then the solution is vertically reflected when choosing the surface tensions $\sigma_{01} = b$ and $\sigma_{12} = a$ and density $\rho_1 = \rho_2 - d$. We show an example of this in Figure 12.

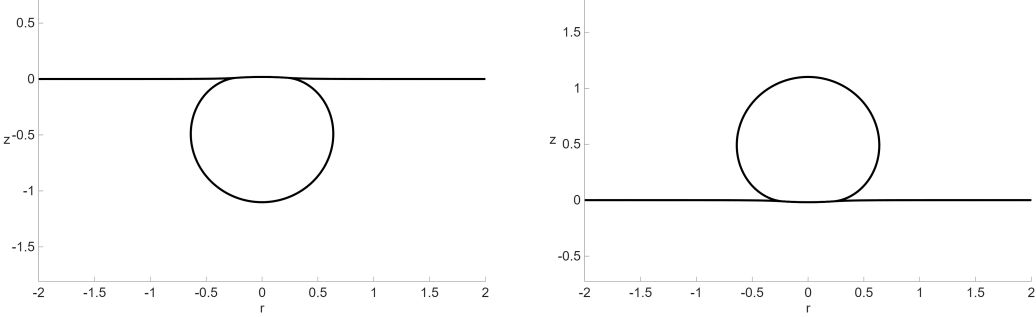


Figure 12: Here are two drops displaying a reflection symmetry of in the parameters. For both drops, the volume is 1, tube radius of $R = 2$, the density of E_2 is $\rho_2 = 15$, a common surface tension of $\sigma_{02} = 6$, and plate angle $\gamma_{0p}^2 = \pi/2$. On the left $\rho_1 = 14.9$, $\sigma_{01} = 7.9999$, $\sigma_{12} = 2.0001$. On the right $\rho_1 = 0.1$, $\sigma_{01} = 2.0001$, $\sigma_{12} = 7.9999$.

4 Floating drops in \mathbb{R}^2

Here we discuss the remaining details needed to formulate the potential energy for configurations in \mathbb{R}^2 . In the following subsections, among other results, we give a parameter study we omitted when we considered floating drops in \mathbb{R}^3 , we show how the heuristic guide of the concavity driving whether the centrally located drop is the energy minimizer is false in general, and we conclude with examples that highlight symmetry breaking.

In Subsection 2.5 the details of computing floating drops in \mathbb{R}^2 were finished. In order to compute the energy of these configurations, we need three quantities: surface area, wetted area (if any), and gravitational potential. The surface area of an interface here is merely the total length of the generating curve, given by 2ℓ , and output by the solver as a part of obtaining the interface. Then multiplying that quantity by the appropriate surface tension gives the potential energy due to surface tension for that interface. As before, the wetting energy of any liquid wetting a wall is obtained by using the height of the interface there. In this case, the height above the reference height $z \equiv 0$ there is simply multiplied by an appropriate physical constant. For the gravitational potential, a generic formula is given by

$$G = \int_a^b \rho g \operatorname{sgn}(w) w^2 dr = \int_{-\ell}^{\ell} \rho g \operatorname{sgn}(w) w^2 \cos \psi ds \quad (35)$$

for some generic $a < b$ and an appropriate density ρ . As before, the form on the left assumes the interface is a graph over B , but the form on the right is given by a parametrization by arc-length, and holds in the parametric form despite the details being omitted here. These quantities are computed from the Chebyshev points along the interface obtained from the solver, and as before, the Clenshaw-Curtis quadrature weights are employed to compute the integrals. With these details in hand, we are able to compute the potential energy for the configurations we consider.

4.1 More parameter space explorations

First, we return to the heuristic that we explored in the last section. There we showed the generally typical behavior that if there is no drop present in the capillary tube and the surface is concave up, then adding a floating drop results in a centrally located drop obtaining lower energy than the wall-bound drop. In Figure 13 we show a parameter study where γ_{0p}^2 is given over a range of values. The usual phenomena occurs where the energy profiles cross at a value of $\pi/2$, but on the left side of the figure the curves cross an additional time. This gives a counter example to the heuristic, and Figure 14 shows

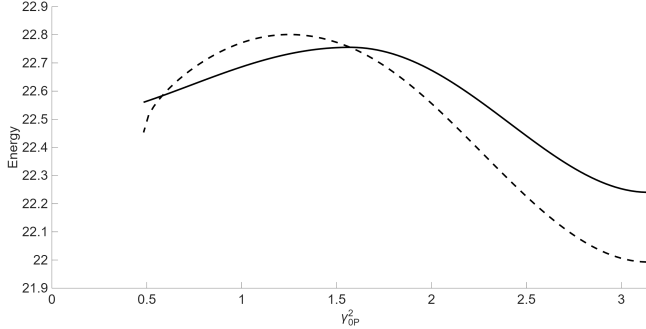


Figure 13: Here is a range of plate angles γ_{0p}^2 where the heuristic breaks. On the left there is an atypical second crossing of the curves away from $\pi/2$. The physical parameters that determine these are volume of 0.4, tube radius of $R = 2$, densities $\rho_1 = 5$ and $\rho_2 = 15$, surface tensions $\sigma_{01} = 7.9999$, $\sigma_{02} = 2.0001$, and $\sigma_{12} = 6$. One plate angle is fixed as $\gamma_{0p}^1 = 2.1277$, and the third is determined by the governing equation.

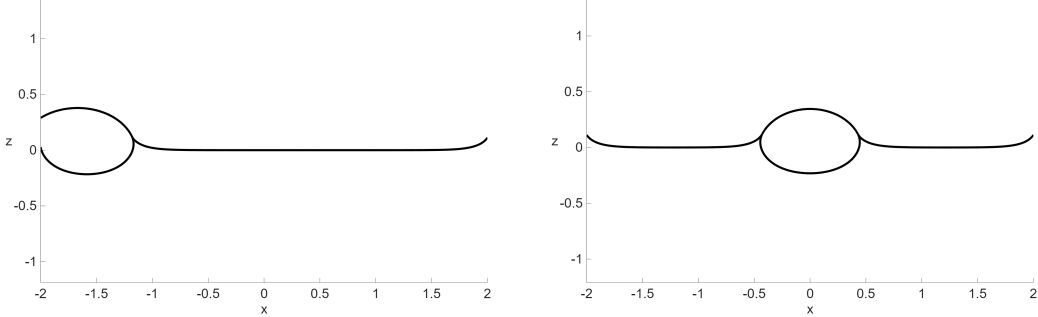


Figure 14: The wall-bound drop displayed here has lower energy than the displayed centrally located drop. Here $\gamma_{0p}^2 = 0.56$ is near the left edge of the experiment in Figure 13.

drops from the unexpected region on the left. It should be pointed out that values of γ_{0p}^2 less than those shown in Figure 13 are not possible, as the governing equation (4) is not solvable there. While our heuristic might be a generally useful guiding intuition, the interplay between the physical parameters is more subtle than this simple parameter test suggests. We have not found a sharp criterion that indicates when such an unexpected phenomena might occur.

In our next example, we consider a variation in the surface tensions. We exhibit this by taking a range of γ_{02} , which is the contact angle on the interior of the drop. As that angle goes to zero, and generally without ever achieving 0, the fixed-volume floating drop problem will limit to a layer of the drop covering the entire tube diameter. In Figure 15 we show energy profiles for centrally located drops, wall-bound drops, and evenly split volumes of wall bound drops attached to each wall.

We end this subsection with an example where another plate angle is varied. With $\gamma_{0p}^2 = \pi/2$ fixed, γ_{0p}^1 is varied, and this is shown in Figure 16. Here the drop split evenly against each wall can be seen to be the minimizer for a range of γ_{0p}^1 on the left.

4.2 Symmetry and asymmetry

The most important question we address for floating drops in \mathbb{R}^2 is that of symmetry. In this setting we have the tools at hand to compute centrally located drops, drops bound to a single wall, and drops split

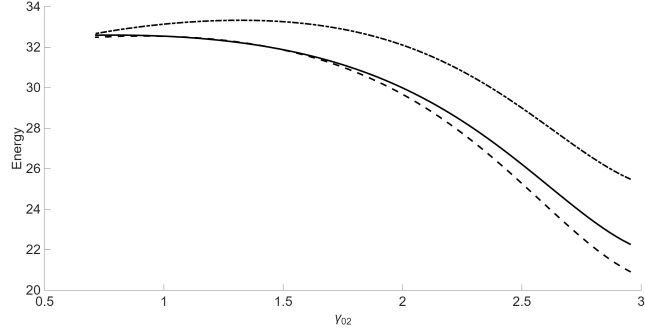


Figure 15: Here is an experiment where γ_{02} is varied over a range of values. The solid curve is the energy of the centrally located drop, the dashed curve is for the wall-bound drop, and the dot-dashed curve is for the drop split evenly on each wall. The physical parameters that determine these are a drop volume of 0.4, a tube radius $X = 2$, densities $\rho_1 = 7.5$ and $\rho_2 = 15$, plate angles $\gamma_{0p}^2 = \pi/2$ and $\gamma_{2p}^1 = 1.252$, and the surface tensions range over the following values in this experiment as $\sigma_{01} \in [2.2, 7.8]$, $\sigma_{02} \in [2.2, 7.8]$, and $\sigma_{12} = 6$.

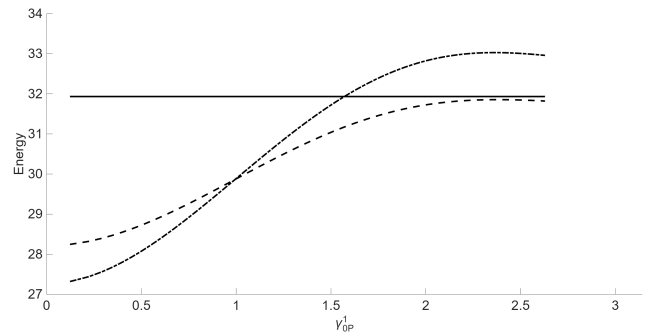


Figure 16: Here is an experiment where γ_{0p}^1 is varied over a range of values. The solid curve is the energy of the centrally located drop, the dashed curve is for the wall-bound drop, and the dot-dashed curve is for the drop split evenly on each wall. The physical parameters that determine these are a total volume of 0.4, a tube radius of $X = 2$, densities of $\rho_1 = 1$ and $\rho_2 = 15$, surface tensions $\sigma_{01} = 3$, $\sigma_{02} = 7$, and $\sigma_{12} = 6$, and the plate angle γ_{0p}^2 is fixed at $\pi/2$ while γ_{1p}^2 is in a range of [1.12, 2.09], generating the displayed third plate angle.

and adjacent to both walls. The configurations that we do not discuss are off-center drops that do not touch a wall as well as split drops that do not touch a wall. Reflection arguments make the off-center drops unlikely to be energy minimizing, and it is not clear that they lead to solvable Euler-Lagrange equations. Split drops that do not meet the wall, and versions of those configurations with multiple drop components not meeting the wall also seem unlikely to be energy minimizing and also may not have solvable Euler-Lagrange equations. So we consider four types of configurations, where our split drops could be evenly or unevenly divided.

In our first example, we consider a configuration where the single wall-bound drop is the energy minimizer. This is shown in Figure 17, where the centrally located drop is also displayed. Then in Figure 18 split drops are shown, with the evenly split drop appearing on the left, and an asymmetric split drop configuration on the right. These asymmetrically split drops have never been observed to be energy minimizers, as one of the other three configurations shown has always produced a lower value of the potential energy. Figure 19 shows the energy profile as the volume is shifted from the right side

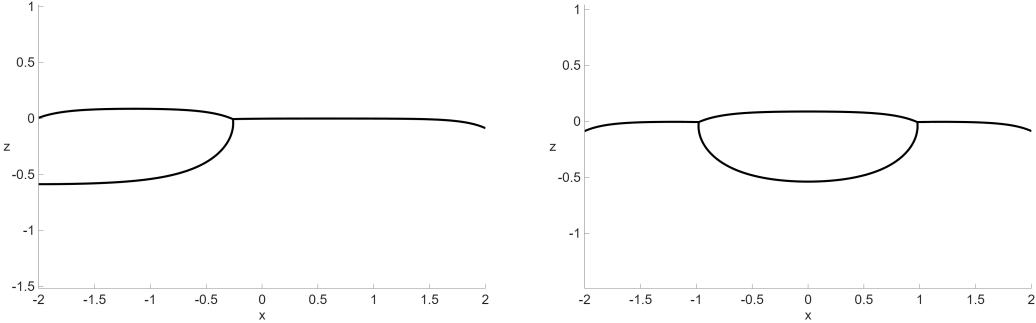


Figure 17: Floating drop configurations with a volume of 1, tube radius of $X = 2$, densities $\rho_1 = 13$ and $\rho_2 = 15$, surface tensions $\sigma_{01} = 7, \sigma_{02} = 6$, and $\sigma_{12} = 3$, and plate angles $\gamma_{0p}^2 = 2$, and $\gamma_{1p}^2 = \pi/2$. On the left is a drop adjacent to the left wall and this is the energy minimizer. On the right is a centrally located drop.

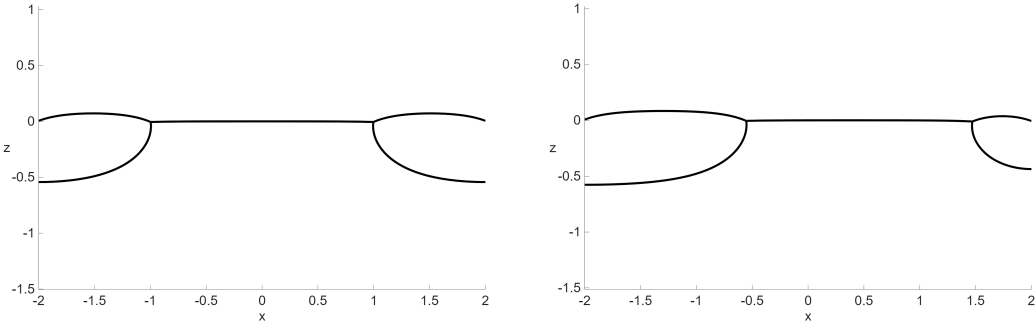


Figure 18: Floating drop configurations with the same physical parameters. On the left is a drop adjacent to the left wall, and this is the energy minimizer. On the left is a drop evenly split between two volumes attached to each wall, and on the right is an unevenly split drop with $1/5$ th the volume adjacent to the right wall.

of the tube to the left side of the tube. It should be emphasized that this is an example of symmetry breaking in that the asymmetric floating drop configuration shown here is observed to be the energy minimizer.

In our second example, we consider a configuration where the evenly split wall-bound drop is the energy minimizer. This is shown in Figure 20, where the centrally located drop is also displayed. Then in Figure 21 split drops are shown, with the evenly split drop appearing on the left, and an asymmetric split drop configuration on the right. Figure 22 shows the energy profile as the volume is shifted from the right side of the tube to the left side of the tube.

4.3 Examples of multiple equal-energy configurations

Finally, we show in Figure 23 a density experiment where there are three values of ρ_1 where the wall-bound drop and the centrally located drop have the same energy value. We are able to find many cases with this number of equal-energy examples, and in Figure 24 we show a range of two parameters where the curves trace out trajectories where the energies are equal. This shows that for some values of ρ_1 there are one, two, or three values of γ_{02} that have equal energy values. It would be possible to run these experiments for different choices of pairs of parameters.

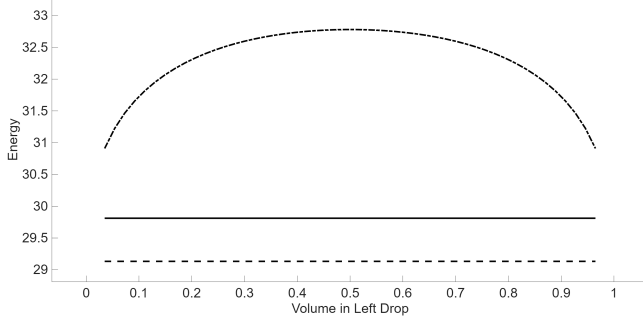


Figure 19: The energy of the split volume drops with the portion of the volume on the left side parameterizing the configurations. The energy of the split volume configurations are shown by a dashed curve, and the solid (constant) curve is the energy of the centrally located drop.

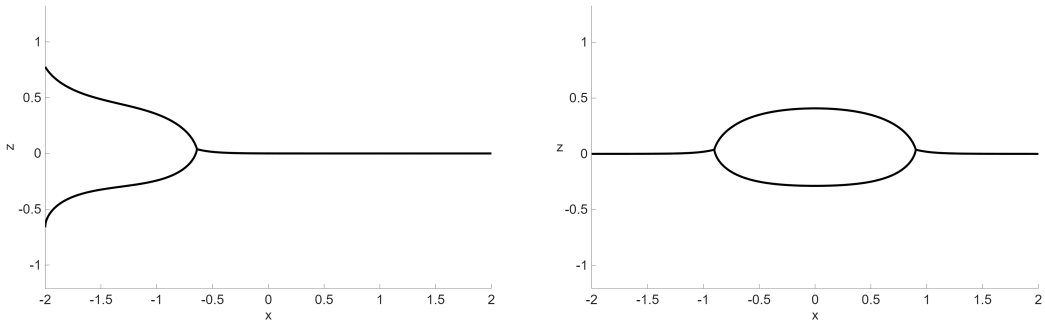


Figure 20: Floating drop configurations with a volume of 1, tube radius of $X = 2$, densities $\rho_1 = 6$ and $\rho_2 = 15$, surface tensions $\sigma_{01} = 7$, $\sigma_{02} = 3$, and $\sigma_{12} = 6$, and plate angles $\gamma_{0p}^2 = \pi/2$, and $\gamma_{1p}^2 = \pi - 0.01$. On the left is a drop adjacent to the left wall. On the right is a centrally located drop.

5 Conclusions

We have considered floating drops that can be described by configurations based on ordinary differential equations. These configurations lead to centrally located drops and symmetric wall-bound drops in \mathbb{R}^3 and additionally when we consider the lower-dimensional problem, we are able to find asymmetric wall-bound drops with either the entire drop volume on one wall, or unevenly split drops adjacent to both walls. In all of these situations, for any given set of physical parameters we are able to find the two distinct floating drops in \mathbb{R}^3 and three distinct floating drops in \mathbb{R}^2 in addition to the one-parameter family of a volume of fluid split between two drops adjacent to each wall. The solutions of the Euler-Lagrange equations for the floating drop problem exhibit no uniqueness at all.

We then explored the potential energy of these different configurations, and we reported on cases where the centrally located drop was the energy minimizer, the symmetric wall-bound drop was the energy minimizer, and the asymmetric wall-bound drop was the minimizer in \mathbb{R}^2 , giving symmetry breaking. In no cases we explored in \mathbb{R}^2 did we find the asymmetric split-drop minimized the energy. We did find many cases where the (presumed) energy minimizer was non-unique. While we do not classify all possible configurations, the examples in \mathbb{R}^2 are likely to exhaust reasonable competitive options. In \mathbb{R}^3 , the asymmetric solutions would involve systems of nonlinear elliptic PDEs, and the numerical methods to treat these free-boundary problems are outside of the scope of this work. It would be interesting to revisit these examples if a robust accurate numerical method was developed that could

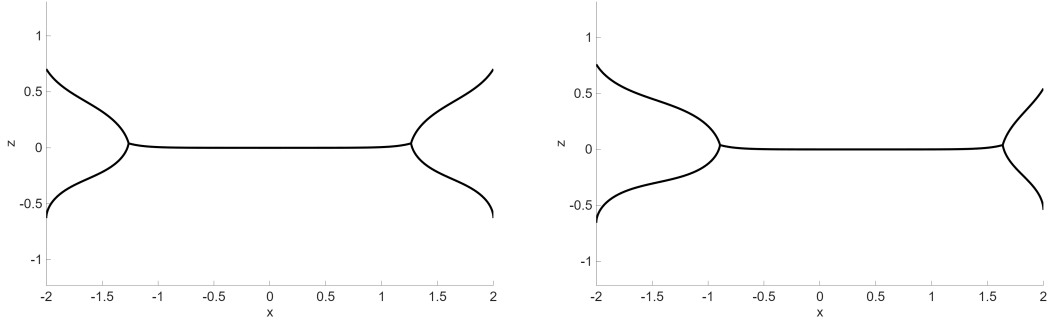


Figure 21: Floating drop configurations with the same physical parameters as Figure 20. On the left is a drop evenly split between two volumes attached to each wall, and this is the energy minimizer. On the right is an unevenly split drop with 1/5th the volume adjacent to the right wall.

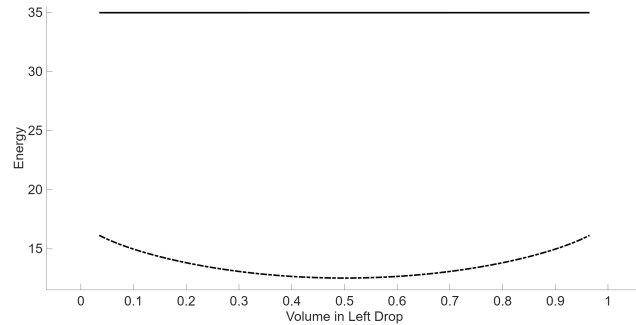


Figure 22: The energy of the split volume drops with the portion of the volume on the left side parameterizing the configurations. The energy of the split volume configurations are shown by a dashed curve, and the solid (constant) curve is the energy of the centrally located drop.

treat some of the subtleties of the capillary equations in more general domains.

We gave guiding heuristics for when a centrally located drop is likely to be the energy minimizer, and we also gave an example of when this is false. We gave an example of when the symmetric split-wall drop is the energy minimizer, and we gave evidence for our findings that the asymmetrical split-wall drop is never the energy minimizer in \mathbb{R}^2 .

In our explorations of this nine-dimensional parameter space, we found four types of energy parameters, those being the bulk parameters of volume and tube radius, density values, surface tensions, and wetting parameters. We gave examples of parameter studies in each of these families. Specifically, we also gave a framework for a volume parameter study that could lead to verification with physical experiments. We observed that some symmetry in certain parameters lead to a reflection symmetry in the drop profile. Finally, we gave some indication to how the parameter space could be further explored by looking at pairs of parameters and classifying the number of equal energy cases found.

As we stated earlier in the paper, we make no claim to have exhausted all of the interesting cases in this somewhat large parameter space. We have merely given a glimpse into the complexity of these problems with our numerical techniques.

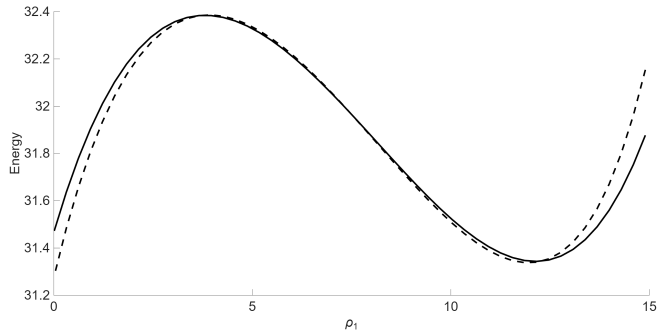


Figure 23: Comparing the energies of the centrally located drop (solid) and the wall-bound drop (dashed). There are three intersections of these curves in the displayed range. The physical parameters are a volume of 0.4 in a tube of radius $X = 2$, densities $\rho_1 = 7.5$ and $\rho_2 = 15$, surface tensions $\sigma_{01} = 3$, $\sigma_{02} = 7$, and $\sigma_{12} = 6$, and plate angles $\gamma_{0p}^2 = \pi/2$ and $\gamma_{1p}^2 = 1.252$.

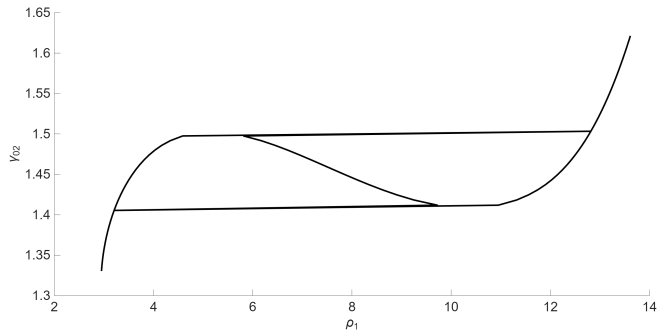


Figure 24: An overview of parameter studies where the number of configurations with equal energy is highlighted. The physical parameters here are a volume of 0.4, a tube radius of $X = 2$, density $\rho_2 = 15$, plate angles $\gamma_{0p}^2 = \pi/2$ and $\gamma_{2p}^1 = 1.252$, and the surface tension $\sigma_{12} = 6$, while σ_{01} ranges over [2.8, 3.2] to produce the range of γ_{02} displayed.

References

- [1] Jared L. Aurentz and Lloyd N. Trefethen, *Block operators and spectral discretizations*, SIAM Rev. **59** (2017), no. 2, 423–446, DOI 10.1137/16M1065975. MR3646500
- [2] Zachary Bagley and Ray Treinen, *On the classification and asymptotic behavior of the symmetric capillary surfaces*, Exp. Math. **27** (2018), no. 2, 215–229, DOI 10.1080/10586458.2016.1245641. MR3798195
- [3] Francis Bashforth and Adams. J.C., *An attempt to test the theories of capillary action by comparing the theoretical and measured forms of drops of fluid*, Cambridge, 1883.
- [4] Ivan Blank, Alan Elcrat, and Raymond Treinen, *Geometry of the triple junction between three fluids in equilibrium*, Electron. J. Differential Equations (2019), Paper No. 101, 35. MR4012582
- [5] Tobin A. Driscoll and Nicholas Hale, *Rectangular spectral collocation*, IMA J. Numer. Anal. **36** (2016), no. 1, 108–132, DOI 10.1093/imanum/dru062. MR3463435
- [6] T. A. Driscoll, N. Hale, and L. N. Trefethen (eds.), *Chebfun Guide*, Pafnuty Publications, Oxford, 2014.
- [7] Alan Elcrat, Tae-Eun Kim, and Ray Treinen, *Annular capillary surfaces*, Arch. Math. (Basel) **82** (2004), no. 5, 449–467, DOI 10.1007/s00013-003-0101-0. MR2061451
- [8] Alan Elcrat, Robert Neel, and David Siegel, *Equilibrium configurations for a floating drop*, J. Math. Fluid Mech. **6** (2004), no. 4, 405–429.
- [9] Alan Elcrat and Ray Treinen, *Numerical results for floating drops*, Discrete Contin. Dyn. Syst. **suppl.** (2005), 241–249.

[10] Alan Elcrat and Ray Treinen, *Floating drops and functions of bounded variation*, Complex Anal. Oper. Theory **5** (2011), no. 1, 299–311, DOI 10.1007/s11785-009-0032-2. MR2773068

[11] Robert Finn, *Equilibrium capillary surfaces*, Grundlehren der Mathematischen Wissenschaften [Fundamental Principles of Mathematical Sciences], vol. 284, Springer-Verlag, New York, 1986.

[12] ———, *The contact angle in capillarity*, Phys. Fluids **18** (2006), no. 4, 047102, 7, DOI 10.1063/1.2185655. MR2259293

[13] S.T. Gibbs, *Ph.D. Thesis Research Proposal*, University of Waterloo (1989).

[14] James Gordon and David Siegel, *Properties of annular capillary surfaces with equal contact angles*, Pacific J. Math. **247** (2010), no. 2, 353–370, DOI 10.2140/pjm.2010.247.353. MR2734153

[15] ———, *Approximating annular capillary surfaces with equal contact angles*, Pacific J. Math. **247** (2010), no. 2, 371–387, DOI 10.2140/pjm.2010.247.371. MR2734154

[16] Jonas Haug and Ray Treinen, *Multi-scale spectral methods for bounded radially symmetric capillary surfaces*, Electron. Trans. Numer. Anal. **60** (2024), 20–39, DOI 10.1553/etna.vol60s20. MR4695961

[17] Henry Ickes and Ray Treinen, *The existence of an energy minimizing configuration for multiple solid objects floating in a bath of three liquids*, Ann. Mat. Pura Appl. (4) **199** (2020), no. 2, 821–831, DOI 10.1007/s10231-019-00902-4. MR4079662

[18] Marquis de La Place, *Celestial mechanics. Vols. I–IV*, Translated from the French, with a commentary, by Nathaniel Bowditch, Chelsea Publishing Co., Inc., Bronx, N.Y., 1966.

[19] Gary Lawlor and Frank Morgan, *Paired calibrations applied to soap films, immiscible fluids, and surfaces or networks minimizing other norms*, Pacific J. Math. **166** (1994), no. 1, 55–83.

[20] Gian Paolo Leonardi, *Infiltrations in immiscible fluids systems*, Proc. Roy. Soc. Edinburgh Sect. A **131** (2001), no. 2, 425–436, DOI 10.1017/S0308210500000937. MR1830418

[21] Francesco Maggi, *Sets of finite perimeter and geometric variational problems*, Cambridge Studies in Advanced Mathematics, vol. 135, Cambridge University Press, Cambridge, 2012. An introduction to geometric measure theory. MR2976521

[22] U. Massari, *The parametric problem of capillarity: the case of two and three fluids*, Astérisque **118** (1984), 197–203 (English, with French summary).

[23] John McCuan, *New geometric estimates for Euler elastica*, J. Elliptic Parabol. Equ. **1** (2015), 387–402, DOI 10.1007/BF03377387. MR3487343

[24] ———, *Self-intersection of nod(oid)al curves*, Geom. Dedicata **216** (2022), no. 6, Paper No. 70, 20, DOI 10.1007/s10711-022-00715-5. MR4487570

[25] John McCuan and Ray Treinen, *Capillarity and Archimedes’ principle of flotation*, Pacific J. Math. **265** (2013), no. 1, 123–150, DOI 10.2140/pjm.2013.265.123. MR3095116

[26] ———, *On floating equilibria in a laterally finite container*, SIAM J. Appl. Math. **78** (2018), no. 1, 551–570, DOI 10.1137/16M1088818. MR3765926

[27] Frank Morgan, *Immiscible fluid clusters in \mathbf{R}^2 and \mathbf{R}^3* , Michigan Math. J. **45** (1998), no. 3, 441–450, DOI 10.1307/mmj/1030132292.

[28] ———, *Geometric measure theory*, 5th ed., Elsevier/Academic Press, Amsterdam, 2016. A beginner’s guide; Illustrated by James F. Bredt. MR3497381

[29] David Siegel, *Approximating symmetric capillary surfaces*, Pacific J. Math. **224** (2006), no. 2, 355–365, DOI 10.2140/pjm.2006.224.355. MR2231935

[30] L.A. Slobozhanin, *Equilibrium and stability of three capillary surfaces with a common line of contact*, Izvestiya Akademii Nauk SSSR, Mekhanika Zhidkosti i Gaza **176** (1986), no. 3, 170–173.

[31] Lloyd N. Trefethen, *Spectral methods in MATLAB*, Software, Environments, and Tools, vol. 10, Society for Industrial and Applied Mathematics (SIAM), Philadelphia, PA, 2000. MR1776072

[32] ———, *Approximation theory and approximation practice*, Society for Industrial and Applied Mathematics (SIAM), Philadelphia, PA, 2013. MR3012510

[33] Ray Treinen, *A general existence theorem for symmetric floating drops*, Arch. Math. (Basel) **94** (2010), no. 5, 477–488.

[34] ———, *Extended annular capillary surfaces*, J. Math. Fluid Mech. **14** (2012), no. 4, 619–632, DOI 10.1007/s00021-012-0100-7. MR2992032

[35] ———, *On the symmetry of solutions to some floating drop problems*, SIAM J. Math. Anal. **44** (2012), no. 6, 3834–3847, DOI 10.1137/110855569. MR3023432

[36] ———, *Spectral methods for capillary surfaces described by bounded generating curves*, Appl. Math. Comput. **450** (2023), Paper No. 127886, 17, DOI 10.1016/j.amc.2023.127886. MR4566044

- [37] Raymond Treinen, *Discussion of a uniqueness result in “equilibrium configurations for a floating drop”*, Electron. J. Differential Equations, posted on 2023, Paper No. 32, 11, DOI 10.58997/ejde.2023.32. MR4574300
- [38] Henry C. Wente, *New exotic containers*, Pacific J. Math. **224** (2006), no. 2, 379–398, DOI 10.2140/pjm.2006.224.379. MR2231937
- [39] Brian White, *Existence of least-energy configurations of immiscible fluids*, J. Geom. Anal. **6** (1996), no. 1, 151–161.